JPEDAV (2008) 29:405–413
DOI: 10.1007/s11669-008-9355-3
1547-7037 ©ASM International

Study of Diffusion and Marker Movement in fcc Ag-Au Alloys

Yajun Liu, Lijun Zhang, Di Yu, and Yang Ge

(Submitted March 1, 2008; in revised form June 12, 2008)

On the basis of the published CALPHAD-type thermodynamic parameters, the atomic mobilities of Ag and Au in face-centered cubic (fcc) Ag-Au alloys are critically assessed, where self-diffusion coefficients, impurity diffusion coefficients, tracer diffusion coefficients, interdiffusion coefficients and concentration curves are simultaneously optimized. Good agreements are obtained by comprehensive comparisons between the calculated and experimentally measured values. In addition, the developed mobilities are successfully used to study inert marker movement for one-dimensional and two-dimensional cases. It is believed that the obtained parameters can provide helpful guidance for material designs.

Keywords Ag-Au, Calphad, diffusion, mobility

1. Introduction

Ag and Au atoms have many similar properties, such as lattice constants, electronic structures, and chemical stabilities, resulting in fairly weak interactions when they are alloyed to form a continuous solid solution over the entire concentration range.[1] Ag, Au, and their alloys are frequently used in jewelry, electrical contacts, and brazing alloys. In addition, the Ag-Au binary system can be used as an ideal candidate for theoretical studies.[2] The diffusion-induced Kirkendall effect in solids is very common in various phenomena, such as migration of macroscopic inclusions inside interaction zones, development of diffusion porosity, generation of internal stress, and even deformation of materials on a microscopic sale.[3–7] These processes are of great concern in a wide variety of fields, including composite materials, coatings, welded components, and thin-film electronic devices.

Highly precise mobility databases of alloys are indispensable in the study of diffusion-controlled transformations. In combination with thermodynamic parameters, mobilities can generate intrinsic diffusion coefficients and interdiffusion coefficients, which can be used to predict diffusion-controlled transformations in multicomponent systems. In the CALPHAD-type assessment procedure for diffusion, model parameters for mobilities of different elements in different phases are evaluated from experimental information[8,9], that is, impurity diffusion coefficients, self-diffusion coefficients, tracer diffusion coefficients, interdiffusion coefficients, and concentration curves. Based on the known experimental information, the obtained mobility parameters can be used to extrapolate diffusion coefficients in the composition and temperature regions where experimental data are absent. Studies of diffusion are not only of theoretical interest but also of practical importance.

So far, great efforts have been made on the assessment of thermodynamic parameters, and various thermodynamic databases are established. However, such is not the case for mobility databases to the best of our knowledge, although they are extremely useful to understand how microstructures evolve at high temperatures. The purpose of this work is to evaluate the atomic mobilities of Ag and Au in face-centered cubic (fcc) Ag-Au alloys as a function of temperatures and compositions by the CALPHAD approach.

2. Model Description

For an n-component system, the interdiffusion coefficients, referred to the volume-fixed reference frame, have been given by the following general expression[10]:

$$D_{kj}^{n} = \sum_{i=1}^{n} (\delta_{ki} - x_k) x_i M_i \left(\frac{\partial \mu_i}{\partial x_j} - \frac{\partial \mu_i}{\partial x_n} \right) \quad \text{(Eq 1)}$$

where δ_{ki} is the Kronecker delta ($\delta_{ki} = 1$ if $i = k$, otherwise $\delta_{ki} = 0$); x_i, μ_i, and M_i are the mole fraction, chemical potential, and mobility of element i, respectively; the nth element is chosen as the dependent element. If A is chosen as the dependent element, the interdiffusion coefficient for a fictitious A-B binary system can be written from Eq 1 as:

$$\tilde{D} = D_{BB}^{A} = x_A x_B M_A \left(\frac{\partial \mu_A}{\partial x_A} - \frac{\partial \mu_A}{\partial x_B} \right) - x_A x_B M_B \left(\frac{\partial \mu_B}{\partial x_A} - \frac{\partial \mu_B}{\partial x_B} \right) \quad \text{(Eq 2)}$$

Yajun Liu, Western Transportation Institute, Montana State University, Bozeman, MT 59715; **Lijun Zhang**, State Key Laboratory of Powder Metallurgy, Central South University, Changsha, Hunan 410083, P.R. China; **Di Yu**, American Water Chemicals Inc., Tampa, FL 33619; and **Yang Ge**, Shanghai Institute of Applied Math and Mechanics, Shanghai University, Shanghai 200072, P.R. China. Contact e-mails: pcbook@hotmail.com and gtg116t@prism.gatech.edu.

For a phase that is described by the substitutional solution model, the chemical potentials of A and B can be evaluated by:

$$\left.\begin{aligned}\mu_A &= G_{\mathrm{m}} + \frac{\partial G_{\mathrm{m}}}{\partial x_A} - \left(x_A \frac{\partial G_{\mathrm{m}}}{\partial x_A} + x_B \frac{\partial G_{\mathrm{m}}}{\partial x_B}\right)\\ \mu_B &= G_{\mathrm{m}} + \frac{\partial G_{\mathrm{m}}}{\partial x_B} - \left(x_A \frac{\partial G_{\mathrm{m}}}{\partial x_A} + x_B \frac{\partial G_{\mathrm{m}}}{\partial x_B}\right)\end{aligned}\right\} \quad \text{(Eq 3)}$$

where G_{m} is the molar Gibbs free energy of a substitutional phase. Inserting Eq 3 into Eq 2, one can obtain the interdiffusion coefficient where the chemical potentials are eliminated:

$$\tilde{D} = (x_A M_B + x_B M_A) x_A x_B \left(\frac{\partial^2 G_{\mathrm{m}}}{\partial^2 x_A} + \frac{\partial^2 G_{\mathrm{m}}}{\partial^2 x_B} - 2\frac{\partial^2 G_{\mathrm{m}}}{\partial x_A \partial x_B}\right) \quad \text{(Eq 4)}$$

The temporal and spatial evolution of element A is given by the Fick's law in the mass conservation form as:

$$\frac{\partial x_A}{\partial t} + \nabla \cdot (-\tilde{D} \nabla x_A) = 0 \quad \text{(Eq 5)}$$

From the absolute rate theory, the mobility for element i can be divided into a frequency factor, M_i^0, and an activation enthalpy, Q_i, by[10]:

$$M_i = \frac{1}{RT}\exp\left(\frac{-Q_i + RT\ln(M_i^0)}{RT}\right) = \frac{1}{RT}\exp\left(\frac{\Phi_i}{RT}\right) \quad \text{(Eq 6)}$$

where Φ_i is a composition-dependent property that can be expressed by the Redlich-Kister polynomial:

$$\Phi_i = x_A \Phi_i^A + x_B \Phi_i^B + x_A x_B \sum_r {}^r\Phi_i^{A,B}(x_A - x_B)^r \quad \text{(Eq 7)}$$

where Φ_i^A, Φ_i^B, and ${}^r\Phi_i^{A,B}$ are model parameters to be evaluated from experimental data and may vary linearly with respect to temperatures.

Assuming a monovacancy mechanism, the tracer diffusion coefficients can be correlated to the atomic mobilities by[11]:

$$\left.\begin{aligned}D_A^* &= RTM_A\\ D_B^* &= RTM_B\end{aligned}\right\} \quad \text{(Eq 8)}$$

where D_A^* and D_B^* are the tracer diffusion coefficients for element A and B, respectively.

If the thermodynamic factor is defined by:

$$F = \frac{x_A x_B}{RT}\left(\frac{\partial^2 G_{\mathrm{m}}}{\partial^2 x_A} + \frac{\partial^2 G_{\mathrm{m}}}{\partial^2 x_B} - 2\frac{\partial^2 G_{\mathrm{m}}}{\partial x_A \partial x_B}\right) \quad \text{(Eq 9)}$$

then Eq 4 can be written as:

$$\tilde{D} = (x_A D_B^* + x_B D_A^*) F \quad \text{(Eq 10)}$$

Alternatively, $\tilde{D}$ can be written in terms of the intrinsic diffusion coefficients:

$$\tilde{D} = (x_A D_B^{\mathrm{I}} + x_B D_A^{\mathrm{I}}) \quad \text{(Eq 11)}$$

where the intrinsic diffusion coefficients of A and B are expressed by:

$$\left.\begin{aligned}D_A^{\mathrm{I}} &= D_A^* F\\ D_B^{\mathrm{I}} &= D_B^* F\end{aligned}\right\} \quad \text{(Eq 12)}$$

Atomic mobilities can be sought from various measured data; this is called an inverse problem. A common way of treating an inverse problem is to minimize an error norm defined on the discrepancy between the predicted and measured quantities[12]:

$$\text{error norm} = \sum w_j (\log D_j^{\mathrm{calc}} - \log D_j^{\mathrm{meas}})^2 + \sum w_k (x_k^{\mathrm{calc}} - x_k^{\mathrm{meas}})^2 \quad \text{(Eq 13)}$$

where w_j and w_k are the weighting factors; D_j^{meas} and D_j^{calc} are the measured and calculated jth diffusion coefficient data; x_k^{meas} and x_k^{calc} are the measured and predicted kth concentration data. The summation is taken over all the data for an optimization, during which various diffusion coefficients can be calculated from Eq 8, 10, and 12.

In this study, the optimization is performed in the optimization lab of a commercial finite element package, Comsol Multiphysics. This optimization lab provides a gradient-based constrained optimization route to find the minimum value for a user-defined problem. It should be noted that a subfunction that can solve Eq 5 with given mobility parameters must be provided in the optimization process to calculate the error norm contribution in Eq 13, which can be naturally provided by Comsol Multiphysics due to its powerful capability in dealing with partial differential equations. During the optimization, the model parameters can be conveniently fixed by equating their upper and lower bounds, and the elimination of some experimental data can be done by setting their weighting factors to zero. It should be noted that there are many choices of the model parameters that can reproduce nearly identical experimental results, and the outputs are weakly sensitive to input variations, which is part and parcel of the characteristics of inverse problems. Therefore, one should adjust all the parameters within reasonable orders of magnitude.[13]

The thermodynamic parameters that were used were taken from the assessment of Hassam et al.[14] All the experimental data mentioned below were selected to evaluate the atomic mobilities of Ag and Au in fcc Ag-Au alloys. The mobility parameters for self-diffusion coefficients of Ag and Au have been reported by Ghosh[15] and Wang et al.,[16] respectively. Accordingly, they were adopted for this study. The impurity diffusion coefficients of Ag in Au and Au in Ag were optimized first to obtain the two mobility end-members. Those interaction parameters were then determined from the tracer diffusion coefficients and the interdiffusion coefficients. At last, the concentration profile data were applied, and a good convergence was expected because the parameters evaluated from various diffusion coefficients could be used as reasonable initial values.

3. Experimental Information

Several investigations have been performed to measure the impurity diffusion coefficients of Au in Ag as well as those of Ag in Au. Using ^{198}Au as the tracing element and applying the sectioning method, Jaumot and Sawatzky,[17] Mead and Birchenall,[18] and Mallard et al.[19] measured the impurity diffusion coefficients of Au in pure Ag over different temperature ranges. Using ^{110}Ag as the tracing element, Mallard et al.,[19] Klotsman et al.,[20] and Herzig and Wolter[21] measured the impurity diffusion coefficients of Ag in pure Au by the sectioning method.

By means of the sectioning technique, Mallard et al.[19] measured the Ag and Au tracer diffusion coefficients in Ag-Au alloys with 0, 8, 17, 35, 50, 66, 83, 94, and 100 at.% Au at different temperatures. The authors reported that the limiting error in such measurements was due to the temperature uncertainty rather than the sectioning process. As a result, the Ag and Au tracer diffusion coefficients measured for different temperatures and compositions were reported. Mead and Birchenall[18] measured the tracer diffusion coefficients of Au in 25 at.% Au alloys and 75 at.% Au alloys at various temperatures by the sectioning method. In addition, the impurity diffusion coefficients of Au in Ag at various temperatures were reported. The authors stated that the chemical interdiffusion coefficients were also measured, but were of low accuracy because of the development of porosity. Meyer and Slifkin[22] measured the tracer diffusion coefficients of Ag and Au at 1223 K by the sectioning method. A radioactive tracer, either ^{198}Au or ^{110}Ag, was plated on one end of each couple that was annealed at 1223 K for different time. The tracer diffusion coefficients of Au and Ag as a function of concentrations were reported. Johnson[23] investigated the tracer diffusion coefficients of Au and Ag as well as the chemical diffusion coefficients in 50.8 at.% Ag alloys at various temperatures, where diffusion was studied by chemical analysis and the use of radioactive Au and Ag as tracers.

Seith and Kottmann[24] measured the interdiffusion coefficients of the Ag-Au system at 1173 K over the entire composition range with Ag/Au diffusion couples annealed for 352,800 seconds. The corresponding concentration distribution of Au across the diffusion couple was measured, and the Matano plane was used to determine the interdiffusion coefficients. Balluffi and Seigle[25] investigated the interdiffusion of the Ag-Au system by gas-solid diffusion couples. High-purity Au disks were used, and Ag was supplied from the vapor phase at 1213 K. The interdiffusion coefficients were reported within the concentration range from 40 to 90 at.% Ag.

Dallwitz[26] measured the concentration distribution of Ag in one diffusion couple that was made of pure Ag and pure Au. Inert markers were placed between the two halves of the couple before annealing. The diffusion couple was annealed at 1177.5 K for 172,800 seconds and then sectioned longitudinally. The element distribution was analyzed by the electron microprobe. The information on the Kirkendall marker displacement was also reported by Dallwitz [26] Cornet[27] investigated the mutual diffusion by Ag/Au diffusion couples annealed at 1188 K for 90,000 seconds. In addition to the concentration curve, the displacement of inert markers to trace the movement of lattice planes was also presented by Cornet.[27]

4. Results and Discussion

4.1 Parameter Assessment

Ghosh[15] optimized the mobility parameters for fcc Ag from the reported experimental self-diffusion coefficients. According to the published experimental data on the self-diffusion coefficients, the mobility parameters for fcc Au were assessed by Wang et al.[16] These mobility parameters can reproduce most of the experimental data, and therefore they are adopted in the present work. The mobility parameters finally obtained in this work as well as those from the work of Ghosh[15] and Wang et al.[16] are listed in Table 1. The Ag-Au phase diagram calculated from the thermodynamic parameters of Hassam et al.[14] is given in Fig. 1. The thermodynamic factors calculated for various temperatures are presented in Fig. 2, where all the curves are convex upward, indicating the solid solution is stable at these temperatures.

Figure 3 shows the calculated temperature dependence of Ag impurity diffusion coefficients of in pure Au compared with the experimental data reported by Mallard et al.,[19] Klotsman et al.,[20] and Herzig and Wolter.[21] The calculated values in the present work are in good agreement with the experimental ones. Figure 4 presents the calculated temperature dependence of Au impurity diffusion coefficients in pure Ag along with the experimental information. The calculated values agree well with the experimental data reported by Jaumot and Sawatzky,[17] Mead and Birchenall,[18] and Mallard et al.[19] Comparisons between the calculated and the experimentally measured temperature and concentration dependence of Au and Ag tracer diffusion coefficients in various Ag-Au alloys are presented in Fig. 5, 6, 7, 8 and 9. As can be clearly seen, the calculated results can reproduce most of the reported experimental data. Figure 10 compares the

Table 1 Mobility parameters for the fcc phase in the Ag-Au binary system (all in SI units)

Phase	Model	Mobility	Parameters
fcc	$(Ag,Au)_1(Va)_1$	Ag	$\Phi^{Au}_{Ag} = -169{,}000 - 97.68T$
			$\Phi^{Ag}_{Ag} = -175{,}892 - 93.50T$(a)
			${}^0\Phi^{Ag,Au}_{Ag} = -34{,}686.15 + 22.10T$
			${}^1\Phi^{Ag,Au}_{Ag} = 6316.20$
		Au	$\Phi^{Au}_{Au} = -176{,}600 - 95.70T$(a)
			$\Phi^{Ag}_{Au} = -202{,}078.51 - 77.88T$
			${}^0\Phi^{Ag,Au}_{Au} = -21{,}198.91 + 4.02T$
			${}^1\Phi^{Ag,Au}_{Au} = -5093.59$

(a) Mobility parameters for self-diffusion of Ag and Au are taken from the work of Ghosh[15] and Wang et al.,[16] respectively

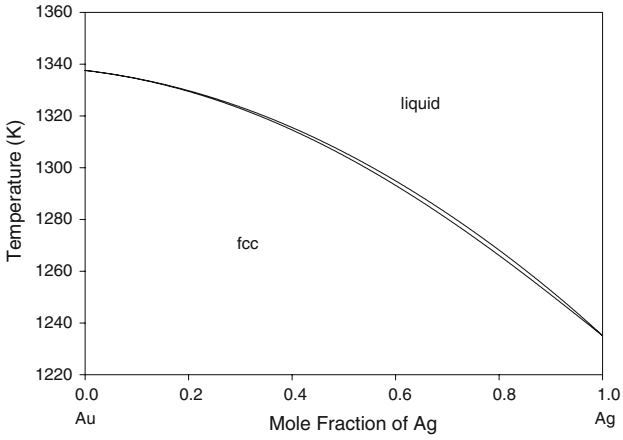

Fig. 1 Calculated Ag-Au binary phase diagram according to the thermodynamic data of Hassam et al.[14]

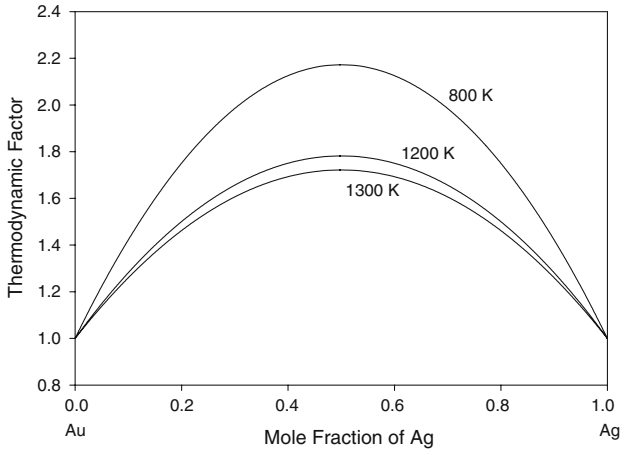

Fig. 2 Calculated thermodynamic factor for various temperatures according to the thermodynamic data of Hassam et al.[14]

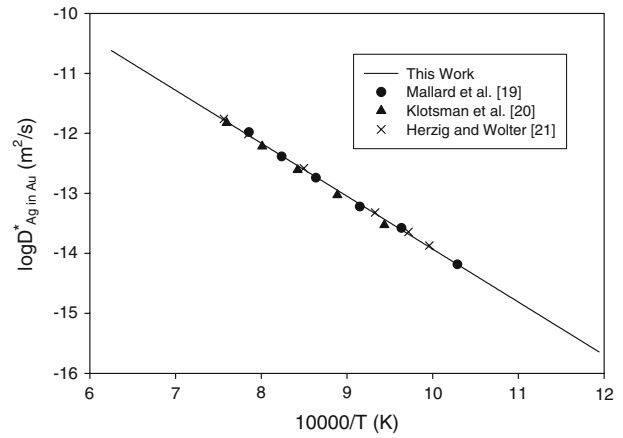

Fig. 3 Calculated and experimentally measured temperature dependence of impurity diffusion coefficients of Ag in Au

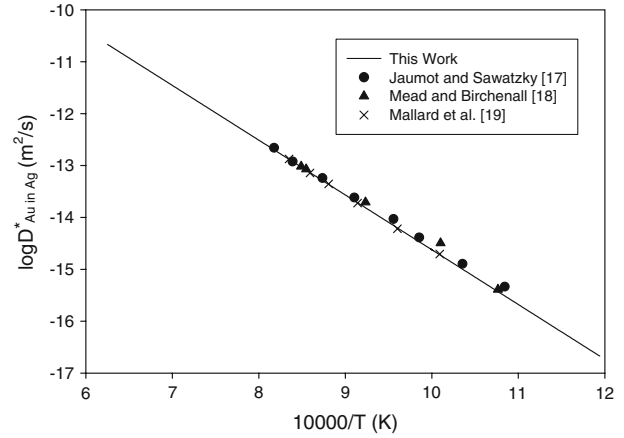

Fig. 4 Calculated and experimentally measured temperature dependence of impurity diffusion coefficients of Au in Ag

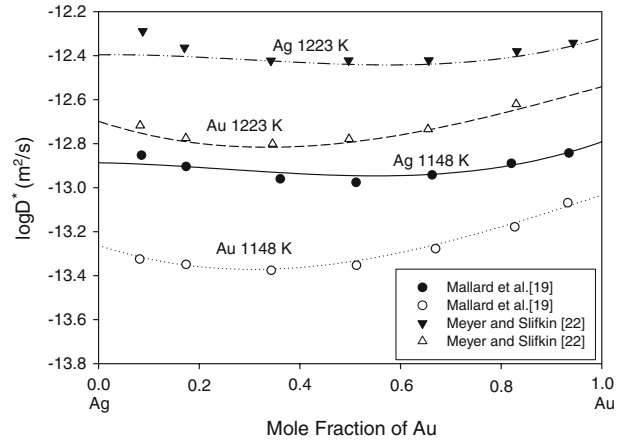

Fig. 5 Comparison between the calculated and experimentally measured tracer diffusion coefficients

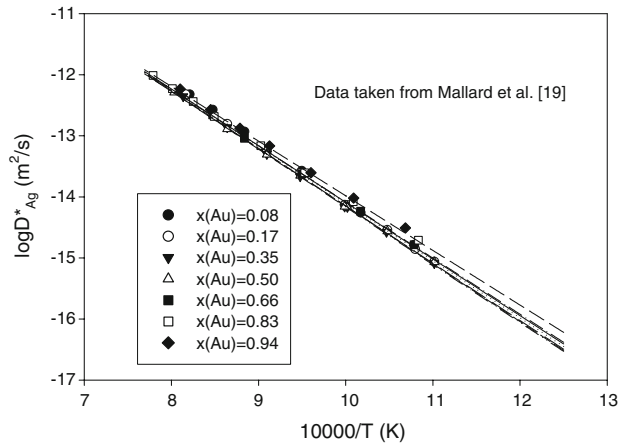

Fig. 6 Comparison between the calculated and experimentally measured Ag tracer diffusion coefficients

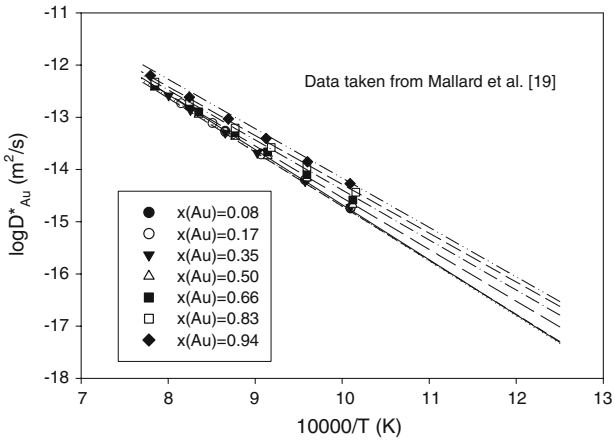

Fig. 7 Comparison between the calculated and experimentally measured Au tracer diffusion coefficients

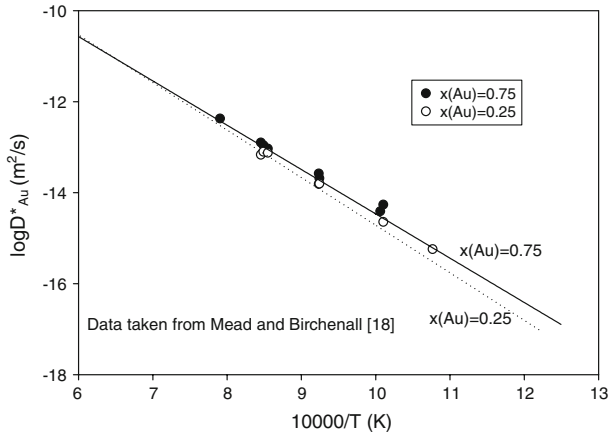

Fig. 8 Comparison between the calculated and experimentally measured Au tracer diffusion coefficients

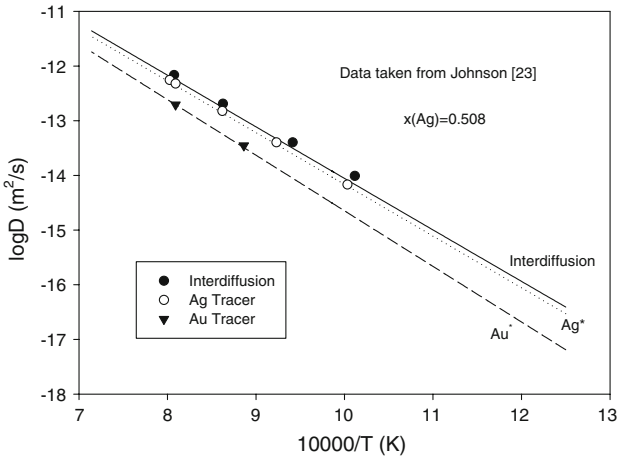

Fig. 9 Comparison between the calculated and experimentally measured various diffusion coefficients

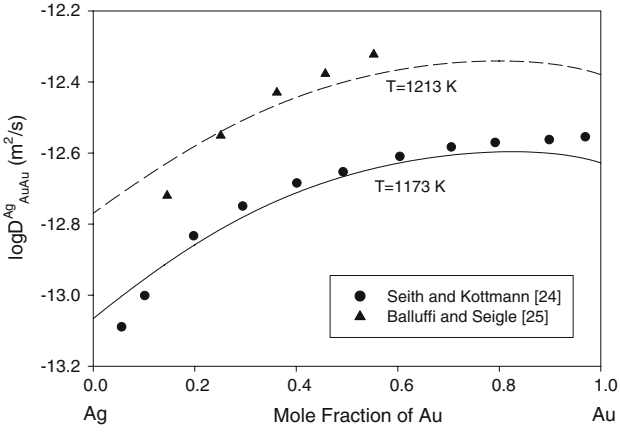

Fig. 10 Comparison between the calculated and experimentally measured interdiffusion coefficients

calculated and experimentally measured interdiffusion coefficients in Ag-Au alloys over the entire composition range. The calculated interdiffusion coefficients are in reasonable agreement with those experimental data.

Figure 11, 12 and 13 present the calculated concentration profiles for Ag/Au diffusion couples, which were annealed at 1188 K for 90,000 seconds, 1173 K for 352,800 seconds, and 1177.5 K for 172,800 seconds, respectively. As shown in the figures, the calculated curves are in good agreement with the experimental data, which confirms the validity of the mobility parameters obtained in this study.

For one-dimensional diffusion problems, the shape of concentration curves and the interdiffusion coefficients are directly correlated. The change of interdiffusion coefficients with respect to compositions can be derived from the curvature of the concentration curves around the Matano plane. Assuming the origin of the coordinate for the concentration curve is placed on the Matano plane and

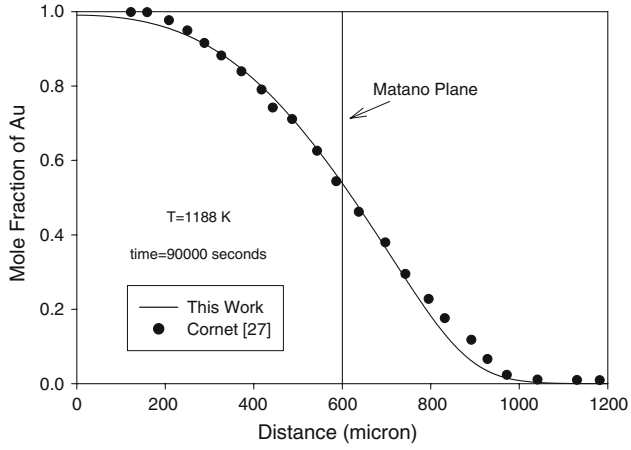

Fig. 11 Comparison between the calculated and experimentally measured concentration profile

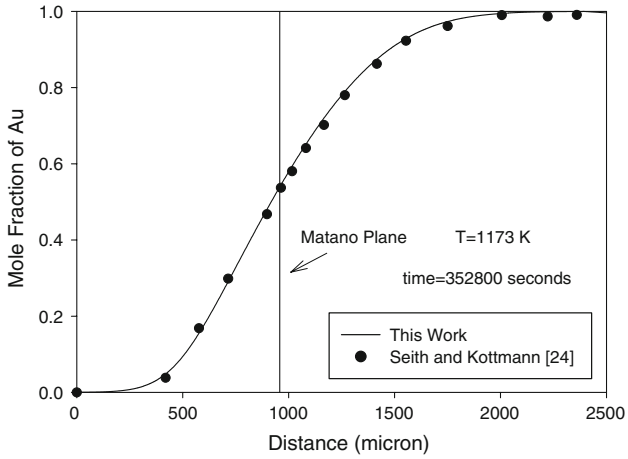

Fig. 12 Comparison between the calculated and experimentally measured concentration profile

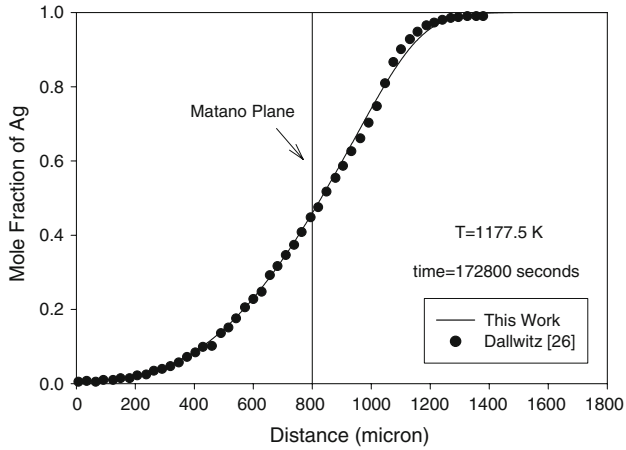

Fig. 13 Comparison between the calculated and experimentally measured concentration profile

applying the Boltzmann transformation, $\lambda = x/\sqrt{t}$, in Eq 5 for one-dimensional diffusion cases, one can have:

$$-\frac{\lambda}{2}\frac{dx_{Ag}}{d\lambda} = \frac{d}{d\lambda}\left[\tilde{D}\frac{dx_{Ag}}{d\lambda}\right] \quad \text{(Eq 14)}$$

where x is the coordinate variable, and x_{Ag} is the Ag molar fraction.

On the Matano plane, $x = 0$ and $\lambda_M = 0$ can be obtained. Therefore, on the Matano plane, Eq 14 can be expressed as:

$$\frac{d}{d\lambda}\left[\tilde{D}\frac{dx_{Ag}}{d\lambda}\right]\Bigg|_{\lambda_M} = 0 \quad \text{(Eq 15)}$$

Upon rearrangement, one has:

$$\left[\frac{d\tilde{D}}{dx_{Ag}}\left(\frac{dx_{Ag}}{d\lambda}\right)^2 + \tilde{D}\frac{d^2x_{Ag}}{d\lambda^2}\right]\Bigg|_{\lambda_M} = 0 \quad \text{(Eq 16)}$$

Equation 16 can also be written as:

$$\left.\frac{d^2x_{Ag}}{d\lambda^2}\right|_{\lambda_M} = -\frac{1}{\tilde{D}}\frac{d\tilde{D}}{dx_{Ag}}\left(\frac{dx_{Ag}}{d\lambda}\right)^2\Bigg|_{\lambda_M} \quad \text{(Eq 17)}$$

Equation 17 states that, on the Matano plane, the curvature of the Ag concentration curve and the change of the interdiffusion coefficients with respect to the Ag concentration should have different signs. In Fig. 13, the curvature on the Matano plane is positive, so it is evident that:

$$\frac{d\tilde{D}}{dx_{Ag}} < 0 \quad \text{(Eq 18)}$$

It can therefore be concluded that the interdiffusion coefficients increase with the concentration of Au around the Matano plane, which can be verified in Fig. 10.

4.2 Marker Movement Simulation

For a binary system, the two constituents may have intrinsic diffusion coefficients that differ significantly from each other, leading to the formation of two unequal and opposite intrinsic fluxes. The occurrence of Kirkendall effect, which is caused by the shift of the crystal lattice during mutual diffusion, can be best visualized by the motion of inert markers placed along the anticipated zone of interdiffusion. Inert markers are frequently used in diffusion studies to trace the movement of lattice planes. Generally speaking, inert markers can be classified into two kinds: Kirkendall markers and non-Kirkendall markers. Kirkendall markers refer to those markers that are placed at the original contact plane where concentration jumps exist, while non-Kirkendall markers are those that are placed at some distance away from the original joining plane with concentration jumps. Therefore, non-Kirkendall markers can only start to move when the concentration front has arrived.

The intrinsic diffusion fluxes of the components, which reflect the mobilities of the species involved in the interaction, are defined with respect to inert markers, the so-called Kirkendall frame of reference. For the binary Ag-Au system, the inert marker velocities in interdiffusion zones can be computed with[28]:

$$\vec{u} = \frac{d\vec{r}}{dt} = (D^I_{Ag} - D^I_{Au})\nabla x_{Ag} \quad \text{(Eq 19)}$$

where $\vec{u}$ and $\vec{r}$ are the velocity and position vectors of each marker, respectively; ∇x_{Ag} is the gradient of the molar fraction of Ag, which has one, two, and three vector components for one-dimensional, two-dimensional, and three-dimensional diffusion problems, respectively. Upon integration, the position of a marker that is placed at $\vec{r}_0$ initially can be calculated by:

$$\vec{r}(\vec{r}_0, t) = \vec{r}_0 + \int_0^t (D^I_{Ag} - D^I_{Au})\nabla x_{Ag} dt \quad \text{(Eq 20)}$$

which shows that the position of a marker depends on not only the difference in intrinsic diffusivities of the species but

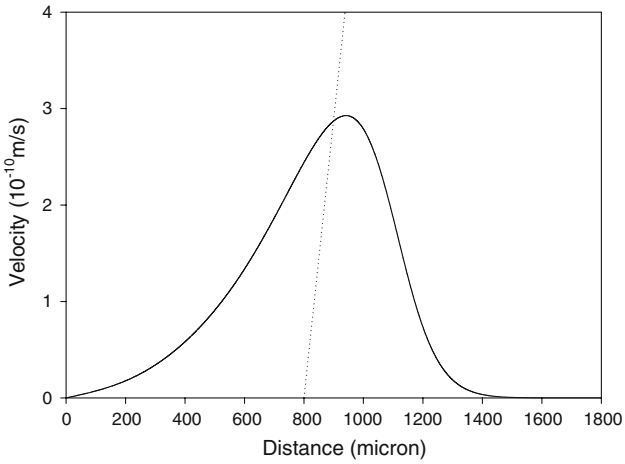

Fig. 14 Graphical construction to determine the Kirkendall Marker position

also the concentration gradient developing in the interdiffusion zone.

For one-dimensional diffusion problems, Kirkendall markers are the only markers that stay at a constant composition and move parabolically with time. Accordingly, instead of using Eq 20 to trace the movement of any marker positioned at $\vec{r}_0$ initially, one may adopt the graphic construction to locate the Kirkendall marker position by the intersection of Eq 19 and 21.[29]

$$\vec{u} = \frac{d\vec{r}}{dt} = \frac{\vec{r}_k}{2t} \qquad \text{(Eq 21)}$$

where $\vec{r}_k$ denotes the displacement between the position of the Kirkendall markers and the Matano plane.

To give confidence in the calculated Kirkendall marker movement, a benchmark example is used where the diffusion couple information is presented in Fig. 13. The author, Dallwitz[26] reported a displacement of about 136 μm. For this one-dimensional diffusion couple, a graphical construction following Eq 19 and 21 is given in Fig. 14, where the intersection point leads to a displacement of around 99 μm for a Kirkendall marker. Considering the difficulties and large experimental errors in marker displacement measurements, such an agreement is satisfactory.

In this work, the movement of Kirkendall markers in a multiple made from two pieces of pure Ag and two pieces of pure Au is investigated. Each piece of Ag or Au has a square dimension of 1600×1600 μm. The four squares are placed with two sides facing each other so that the interfaces form a cross, where inert markers are placed. The temperature and time used for the diffusion simulation can be found in Fig. 13. The simulation setup as well as the final marker distribution is presented in Fig. 15. It can be seen that the inert markers rearrange upon interdiffusion, and all the markers in the diffusion zone are clearly displaced in the Ag direction. Because of the assumption that the volume of the fcc phase is not dependent on concentrations, the four edges of the multiple remain

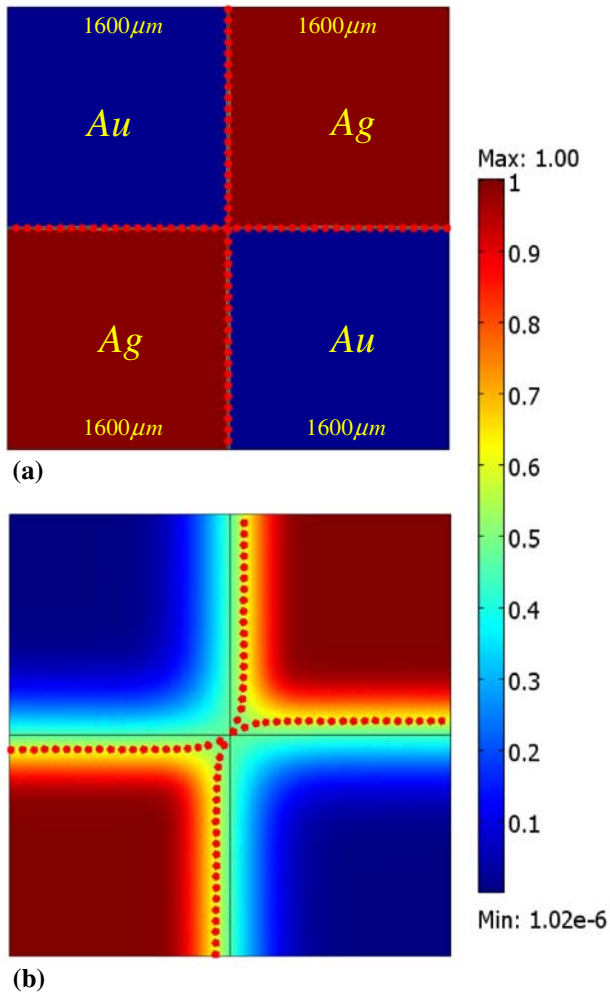

Fig. 15 Simulated Kirkendall marker movement in a diffusion couple annealed at 1177.5 K for 172,800 seconds. (a) Before interdiffusion and (b) after interdiffusion. The color bar denotes the concentration scale for Ag

straight, and the multiple ends do not displace relative to one another. Another interesting feature that can be seen from this plot is the distribution of Kirkendall markers around the center, which are aligned along the Ag-Ag diagonal direction.

As mentioned previously, non-Kirkendall markers are defined as the markers except for Kirkendall ones. In this study, one piece of pure Ag and one piece of pure Au with a dimension of 1600×1600 μm are joined together to investigate the movement of non-Kirkendall markers that are placed along a straight line forming an angle of 45° with the joining plane. The diffusion simulation is made for 1177.5 K and 691,200 seconds. The distribution of markers before and after annealing is given in Fig. 16. Initially, these markers form a straight line, but upon interdiffusion, these markers that are within the interdiffusion zone shift to the Ag side, leading to a notable bend of the marker array in this diffusion couple. It is also noted that the markers out of the interdiffusion zone still remain unchanged, and the marker

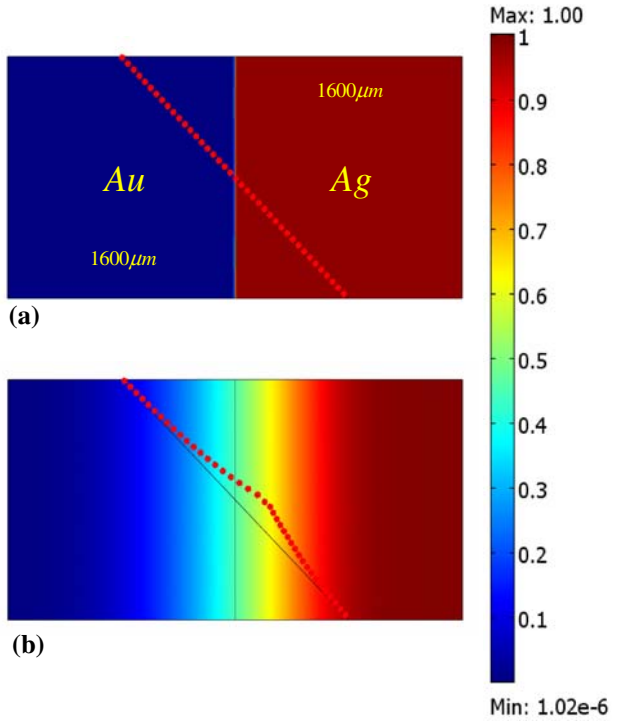

Fig. 16 Simulated non-Kirkendall marker movement in a diffusion couple annealed at 1177.5 K for 691,200 seconds. (a) Before interdiffusion and (b) after interdiffusion. The color bar denotes the concentration scale for Ag

with the largest displacement is the one that is placed nearest to the Matano plane.

5. Conclusions

The atomic mobilities of Ag and Au in fcc Ag-Au alloys have been derived from various experimental data in the literature, including impurity diffusion coefficients, tracer diffusion coefficients, interdiffusion coefficients, and concentration curves. Good agreements are obtained by comprehensive comparisons between the calculated and experimentally measured data. In addition, the developed mobility parameters, in conjunction with CALPHAD-based thermodynamic parameters, have been used to investigate Kirkendall and non-Kirkendall marker movement. The results show that the markers will generally move to the Ag side because of the higher intrinsic diffusion coefficients of Ag.

References

1. G. Bozzolo, J.E. Garcés, and G.N. Derry, Atomistic Modeling of Segregation and Bulk Ordering in Ag-Au Alloys, *Surf. Sci.*, 2007, **601**(9), p 2038-2046
2. F. Seitz, On the Theory of Vacancy Diffusion in Alloys, *Phys. Rev.*, 1948, **74**(10), p 1513-1523
3. I.A. Szabó, G. Opposits, C. Cserhati, and D.L. Beke, The Effect of Stresses on the Selection of the Kirkendall Marker Plane, *Defect Diffus. Forum*, 2003, **216-217,** p 47–52
4. M.J.H. van Dal, A.M. Gusak, C. Cserháti, A.A. Kodentsov, and F.J.J. van Loo, Microstructural Stability of the Kirkendall Plane in Solid-State Diffusion, *Phys. Rev. Lett.*, 2001, **86**(15), p 3352-3355
5. M.J.H. van Dal, M.C.L.P. Pleumeekers, A.A. Kodentsov, and F.J.J. van Loo, Intrinsic Diffusion and Kirkendall Effect in Ni-Pd and Fe-Pd Solid Solutions, *Acta Mater.*, 2000, **48**(2), p 385-396
6. J.S. Kirkaldy and G. Savva, Correlation between Coherency Strain Effects and the Kirkendall Effect in Binary Infinite Diffusion Couples, *Acta Mater.*, 1997, **45**(8), p 3115-3121
7. M.J.H. van Dal, M.C.L.P. Pleumeekers, A.A. Kodentsov, and F.J.J. van Loo, Diffusion Studies and Re-examination of the Kirkendall Effect in the Au-Ni System, *J. Alloys Compd.*, 2000, **309**(1-2), p 132-140
8. Y.W. Cui, K. Oikawa, R. Kainuma, and K. Ishida, Study of Diffusion Mobility of Al-Zn Solid Solution, *J. Phase Equilib. Diffus.*, 2006, **27**(4), p 333-342
9. C.E. Campbell, W.J. Boettinger, and U.R. Kattner, Development of a Diffusion Mobility Database for Ni-base Superalloys, *Acta Mater.*, 2002, **50**(4), p 775-792
10. T. Helander and J. Ågren, Diffusion in the B2-B.C.C. Phase of the Al-Fe-Ni System-Application of a Phenomenological Model, *Acta Mater.*, 1999, **47**(11), p 3291-3300
11. T. Helander and J. Ågren, A Phenomenological Treatment of Diffusion in Al-Fe and Al-Ni Alloys Having B2-BCC Ordered Structure, *Acta Mater.*, 1999, **47**(4), p 1141-1152
12. C.E. Campbell, A New Technique for Evaluating Diffusion Mobility Parameters, *J. Phase Equilib. Diffus.*, 2005, **26**(5), p 435-440
13. Y. Liu and D. Liang, Comment on "Diffusion Mobilities for the B2-bcc Phase in the Ni-Al Binary System", *J. Alloys Compd.*, 2008, **459**(1-2), p L5-L7
14. S. Hassam, J. Ågren, M. Gaune-Escard, and J.P. Bros, The Ag-Au-Si System: Experimental and Calculated Phase Diagram, *Metall. Trans. A*, 1990, **21**, p 1877-1884
15. G. Ghosh, Dissolution and Interfacial Reactions of Thin-Film Ti/Ni/Ag Metallizations in Solder Joints, *Acta Mater.*, 2001, **49**, p 2609-2624
16. J. Wang, L.B. Liu, H.S. Liu, and Z.P. Jin, Assessment of the Diffusional Mobilities in the Face-Centred Cubic Au-Ni Alloys, *CALPHAD*, 2007, **31**(2), p 249-255
17. F.E. Jaumot and A. Sawatzky, Diffusion of Gold in Single Crystals of Silver, *J. Appl. Phys.*, 1956, **27**(10), p 1186-1188
18. H.W. Mead and C.E. Birchenall, Diffusion in Gold and Au-Ag Alloys, *J. Met.*, 1957, **9**, p 874-877
19. W.C. Mallard, A.B. Gardner, R.F. Bass, and L.M. Slifkin, Self-Diffusion in Silver-Gold Solid Solutions, *Phys. Rev.*, 1963, **129**(2), p 617-625
20. S.M. Klotsman, N.K. Arkhipova, A.N. Timofeev, and I.S. Trakhtenberg, Diffusion of Silver in Polycrystalline Gold, *Phys. Met. Metall.*, 1965, **20**(3), p 70-75
21. C. Herzig and D. Wolter, Isotope-Effect for Diffusion of Silver in Gold, *Z Metallkde.*, 1974, **65**, p 273-278
22. R.O. Meyer and L.M. Slifkin, Activity Coefficient and Vacancy-flow Effects on Diffusion in Silver-Gold Alloys, *Phys. Rev.*, 1966, **149**(2), p 556-563
23. W.A. Johnson, Diffusion Experiments on a Gold-Silver Alloy by Chemical and Radioactive Tracer Methods, *Trans. Am. Inst. Min. Metall. Eng.*, 1942, **147**, p 331-346
24. W. Seith and A. Kottmann, Diffusion in Solid Metals, *Angew. Chem.*, 1952, **64**, p 379-391

25. R.W. Balluffi and L.L. Seigle, Diffusion in Bimetal Vapor-Solid Couples, *J. Appl. Phys.*, 1954, **25**(5), p 607-614
26. M.J. Dallwitz, The Vacancy-Flow Effect in Silver-Gold Alloys, *Acta Metall.*, 1972, **20**, p 1229-1234
27. J. Cornet, A Thorough Study of the Kirkendall Effect According to the Equations of Darken, *J. Phys. Chem. Solids*, 1974, **35**, p 1247-1252
28. R. Bachorczyk, M. Danielewski, and R. Filipek, Kirkendall Shift in Multicomponent Systems, *Solid State Phenomena*, 2000, **72**, p 153-156
29. M.J.H. van Dal, A.M. Gusak, C. Cserháti, A.A. Kodentsov, and F.J.J. van Loo, Spatio-temporal Instabilities of the Kirkendall Marker Planes During Interdiffusion in β′-AuZn, *Philos. Mag. A*, 2002, **82**(5), p 943-954